Journal of Sound and Vibration (1997) **208**(2), 211–224

EXTERNAL PRIMARY RESONANCE OF SELF-EXCITED OSCILLATORS WITH 1:3 INTERNAL RESONANCE

S. Natsiavas and P. Metallidis

Department of Mechanical Engineering, *Aristotle University*, 54006 *Thessaloniki*, *Greece*

(*Received* 7 *May* 1996, *and in final form* 2 *June* 1997)

The forced response of a class of weakly non-linear oscillators with self-excited characteristics is investigated. The non-linearity is symmetric, the external forcing is harmonic and the essential dynamics are described by a two-degree-of-freedom oscillator, whose linear natural frequencies satisfy conditions of 1:3 internal resonance. Firstly, sets of equations governing the slow time variation of the amplitudes and phases of approximate solutions of the equations of motion are obtained by applying an asymptotic analytical method. For primary resonance of the first mode, only mixed-mode response is possible, since the second mode is always activated through the non-linearities. On the other hand, when conditions of primary resonance of the second mode are met, single-mode response is also possible. In both cases, a methodology is developed which reduces the determination of constant solutions of the slow-flow equations to the solution of two coupled polynomial equations. The stability analysis of these solutions is also provided. Next, numerical results are presented for an example practical system, in the form of response diagrams. These results show the effect of some system parameters on the existence and interaction of various branches of constant solutions. Then, more numerical results are presented, obtained by direct integration of the slow-flow equations in forcing frequency ranges where these equations possess no stable constant solution. The results demonstrate the existence of periodic and chaotic solutions of these equations.

1. INTRODUCTION

Modal interactions occurring in the response of non-linear mechanical systems, in the presence of an internal resonance, have been at the epicenter of intensive research work over the last three decades. For such systems, some of the energy supplied to a mode of the system by the excitation may be transferred and activate other modes, participating in the same internal resonance. However, most of these studies analyzed systems with non-linear restoring force only (see [1–8] and references therein). On the other hand, many mechanical oscillators may exhibit significant damping nonlinearities, leading to self-excited behavior (e.g., [9–16]). For such systems, vibration modes which are not excited directly by external forcing may eventually get excited through the non-linearities and mixed-mode response may arise, even in the absence of internal resonance [16, 17].

The main objective of this study is to present an analysis for the forced response of a class of two-degree-of-freedom self-excited oscillators, in the presence of a one-to-three internal resonance. The non-linearity is weak and consists of cubic combinations of displacement and velocity terms. The normalized equations of motion are first presented in a general form in the following section. Next, a perturbation method is applied and a

0022–460X/97/470211 + 14 $25.00/0/sv971145

set of four ordinary differential equations is presented, governing the slow variation of the amplitudes and phases of approximate solutions of the equations of motion for the case of primary resonance of the first mode. A methodology leading to an efficient computation of constant solutions of the averaged equations is then presented, together with an appropriate stabilty analysis. The fourth section includes similar analyses for the case of primary resonance of the second mode. Then, a specific practical example is considered and a series of representative response diagrams is first presented, illustrating the effect of some important system parameters on the existence and interaction of constant solution branches. In the sixth section, results are presented, which are obtained by integrating the slow-flow equations in forcing frequency ranges where these equations possess no stable constant solution. In the final section, the most important conclusions of the study are summarized.

2. DYNAMICAL SYSTEM

The dynamics of the mechanical systems examined in the present work can be described adequately by a set of two coupled non-linear equations of motion, with normalized form:

$$\ddot{u}_n + \omega_n^2 u_n = h_n(\tau) + \varepsilon q_n(u_1, u_2, \dot{u}_1, \dot{u}_2) \qquad (n = 1, 2), \tag{1}$$

where ε is a small positive constant and

$$q_n(u_1, u_2, \dot{u}_1, \dot{u}_2) = \alpha_{n1}\dot{u}_1 + \alpha_{n2}\dot{u}_2 + \beta_{n1}\dot{u}_1^3 + \beta_{n2}\dot{u}_1^2\dot{u}_2 + \beta_{n3}\dot{u}_1\dot{u}_2^2 + \beta_{n4}\dot{u}_2^3 + \gamma_{n1}u_1^3 + \gamma_{n2}u_1^2u_2 + \gamma_{n3}u_1u_2^2 + \gamma_{n4}u_2^3. \tag{2}$$

The coefficients of the coupling functions $q_n(u_1, u_2, \dot{u}_1, \dot{u}_2)$ are such that self-excited response is possible. For instance, this is the case when the constants α_{n1}, α_{n2} are positive.

When no internal resonance is activated, the response of this class of oscillators can be analyzed according to the methodology presented in [17]. Here, that analysis is extended to cover cases where the system examined exhibits one-to-three internal resonance. This means that its undamped linear natural frequencies satisfy the relation

$$\omega_2 = 3\omega_1 + \varepsilon\sigma, \tag{3}$$

where σ is the natural frequency detuning parameter.

An example of a two-degree-of-freedom mechanical system, with equations of motion that can be cast in the form (1) and (2), is shown in Figure 1. This oscillator presents a simplified model of a metal cutting process [12]. The springs and dampers connecting the masses of the model with the ground possess linear characteristics. On the other hand, the spring and damper between the two masses are chosen to possess Duffing and Rayleigh type characteristics, respectively. Therefore, if the relative displacement and velocity of the two masses is x and v, then the force developed between them has the form $(k_0x + \hat{k}_0x^3) + (-c_0v + \hat{c}_0v^3)$. Finally, the external excitation consists of harmonic forces

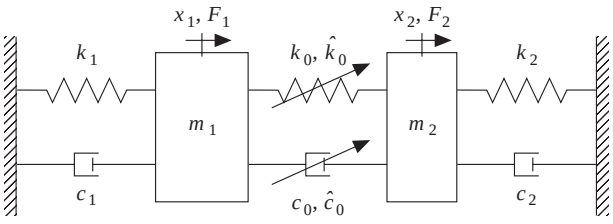

Figure 1. Example of mechanical system model.

$F_1 \cos(\Omega t)$ and $F_2 \cos(\Omega t + \phi)$, applied on the first and second mass of the model, respectively.

The equations of motion of the example system can be brought into the general form of equations (1) and (2) by first introducing the normalized time $\tau = \hat{\omega}_1 t$ and the absolute displacements $y_n = x_n | x_c$, $(n = 1, 2)$. The frequency $\hat{\omega}_1$, the characteristic length x_c and the other system parameters are defined in the Appendix. Then, the process is completed by applying the co-ordinate transformation

$$\mathbf{y}(\tau) = \mathbf{Y}\mathbf{u}(\tau), \tag{4}$$

where $\mathbf{Y}$ is the modal matrix of the corresponding linear, undamped system and by employing standard modal analysis techniques (see [17]). Anticipating conditions of primary external resonance, the normalized forcing terms are also scaled in the form

$$h_n(\tau) = 2\varepsilon p_n \cos(\omega\tau + \theta_n),$$

with amplitudes and phases defined in the Appendix. Finally, the frequency condition (3) is satisfied by proper choice of the parameter ρ.

3. PRIMARY RESONANCE OF THE FIRST MODE

In this section, it is assumed that the forcing frequency lies in the neighborhood of the first undamped linear natural frequency of the dynamical system. This is expressed by the relation

$$\omega = \omega_1 + \varepsilon\sigma_1, \tag{5}$$

where σ_1 is a frequency detuning parameter. For this case, approximate solutions of equations (1) are obtained by applying the multiple time scales method. Namely, these solutions are first expressed in the form:

$$u_n(\tau; \varepsilon) = u_{n0}(\tau, \tau_1) + \varepsilon u_{n1}(\tau, \tau_1) + O(\varepsilon^2), \qquad (n = 1, 2) \tag{6}$$

where $\tau_1 = \varepsilon\tau$ is the slow time scale of the problem. Then, following standard procedures (see [3, 17]), the leading order solution is determined in the form:

$$u_{n0} = a_n(\tau_1) \cos[\omega_n \tau + \phi_n(\tau_1)], \tag{7}$$

where the amplitudes $\alpha_n(\tau_1)$ and phases $\phi_n(\tau_1)$ satisfy the following autonomous system of slow-flow equations:

$$\alpha_1' = c_1\alpha_1 + c_2\alpha_1^3 + c_3\alpha_1\alpha_2^2 + c_4 \sin\gamma_1 + (c_7 \sin\gamma - c_8 \cos\gamma)\alpha_1^2\alpha_2, \tag{8}$$

$$\alpha_1\gamma_1' = \sigma_1\alpha_1 + c_5\alpha_1^3 + c_6\alpha_1\alpha_2^2 + c_4 \cos\gamma_1 + (c_7 \cos\gamma + c_8 \sin\gamma)\alpha_1^2\alpha_2, \tag{9}$$

$$\alpha_2' = e_1\alpha_2 + e_2\alpha_1^2\alpha_2 + e_3\alpha_2^3 - (e_7 \sin\gamma + e_8 \cos\gamma)\alpha_1^3, \tag{10}$$

$$\alpha_2\gamma_2' = \hat{\sigma}_2\alpha_2 + e_5\alpha_1^2\alpha_2 + e_6\alpha_2^3 + (e_7 \cos\gamma - e_8 \sin\gamma)\alpha_1^3. \tag{11}$$

The constant coefficients appearing in the above set of first order ordinary differential equations are defined in the Appendix, while

$$\gamma = \varphi_2 - 3\varphi_1 + \sigma\tau_1, \qquad \gamma_1 = \sigma_1\tau_1 + \theta_1 - \varphi_1, \qquad \gamma_2 = \hat{\sigma}_2\tau_1 - \phi_2 \tag{12a–c}$$

and $\hat{\sigma}_2$ is a constant that will be defined subsequently.

It should be noted that the form of the slow-flow equations is not affected by addition of the remaining possible combinations of cubic terms in the coupling functions expressed by (2). Namely, addition of

$$\mu_{n1}\dot{u}_1^2 u_1 + \mu_{n2}\dot{u}_1^2 u_2 + \mu_{n3}\dot{u}_1\dot{u}_2 u_1 + \mu_{n4}\dot{u}_1\dot{u}_2 u_2 + \mu_{n5}\dot{u}_2^2 u_1 + \mu_{n6}\dot{u}_2^2 u_2$$
$$+ \nu_{n1}u_1^2\dot{u}_1 + \nu_{n2}\dot{u}_1^2 u_2 + \nu_{n3}u_1 u_2\dot{u}_1 + \nu_{n4}u_1 u_2\dot{u}_2 + \nu_{n5}u_2^2\dot{u}_1 + \nu_{n6}u_2^2\dot{u}_2$$

in q_n introduces the terms $\delta_1 - \delta_4$ (which are defined in the Appendix) in equations (8)–(11), respectively. Therefore, the coefficients of these extra terms play a similar role in those equations with that of the coefficients γ_{nm} and β_{nm}, respectively. Moreover, if $(\alpha_1, \alpha_2, \gamma_1, \gamma_2)$ is a solution of equations (8)–(11), then it can be shown that

$$(-\alpha_1, \alpha_2, \pi + \gamma_1, \gamma_2), \qquad (\alpha_1, -\alpha_2, \gamma_2, \pi + \gamma_2), \qquad (-\alpha_1, -\alpha_2, \pi + \gamma_1, \pi + \gamma_2),$$

are also solutions. Finally, it can easily be proved that only *mixed-mode* solutions (i.e., motions with $\alpha_1\alpha_2 \neq 0$) are possible for the system (8)–(11), provided that at least one of the coefficients e_7 and e_8 is not equal to zero.

Among other types of solutions, the slow-flow equations (8)–(11) are expected to possess *constant solutions* $(\alpha_{10}, \alpha_{20}, \gamma_{10}, \gamma_{20})$, satisfying the conditions

$$\alpha_{10}' = \alpha_{20}' = \gamma_{10}' = \gamma_{20}' = \gamma_0' = 0. \tag{13}$$

Then, by employing the definition (12) of the phases, it can be shown that the following conditions must hold:

$$\hat{\sigma}_2 = 3\sigma_1 - \sigma, \qquad \gamma_0 = 3\gamma_{10} - \gamma_{20} - 3\theta_1. \tag{14a, b}$$

As a consequence, by combining condition (14a) with the frequency relations (3) and (5), the approximate solutions expressed by (7) are finally determined in the form

$$u_1 = \alpha_{10}\cos(\omega\tau + \theta_1 - \gamma_{10}) + O(\varepsilon) \tag{15}$$

and

$$u_2 = \alpha_{20}\cos(3\omega\tau - \gamma_{20}) + O(\varepsilon). \tag{16}$$

From the last two equations it is clear that the constant mixed-mode solutions of the averaged equations (8)–(11) correspond to periodic motions of the mechanical system, in contrast to the non-resonant case [17], where the response is two-frequency quasiperiodic. Therefore, in the presence of the 1:3 internal resonance, the non-linearity adjusts the response frequencies of the system so that the three-frequency quasiperiodic response (involving ω, ω_1 and ω_2) is replaced by a two-frequency periodic response.

Determination of the constant mixed-mode solutions $\mathbf{x}_0 = (\alpha_{10}\ \alpha_{20}\ \gamma_{10}\ \gamma_{20})^{\mathrm{T}}$ can be reduced to solution of two polynomial equations. First, application of conditions (13) in (8)–(11) yields a system of four algebraic equations for the four unknowns of the problem. Solving the two algebraic equations resulting from (10) and (11) for $\cos\gamma_0$ and $\sin\gamma_0$ yields expressions with the form:

$$\cos\gamma_0 = (g_1 + g_2 x_1 + g_3 x_2)\alpha_{20}/\alpha_{10}^3, \qquad \sin\gamma_0 = (g_4 + g_5 x_1 + g_6 x_2)\alpha_{20}/\alpha_{10}^3, \tag{17, 18}$$

where $x_1 = \alpha_{10}^2$, $x_2 = a_{20}^2$. Next, substituting (17) and (18) in the algebraic equations resulting from (8) and (9) yields the quantities $\cos\gamma_{10}$ and $\sin\gamma_{10}$ in the form

$$\cos\gamma_{10} = (q_1 x_1 + q_2 x_2 + q_3 x_1^2 + q_4 x_1 x_2 + q_5 x_2^2)/\alpha_{10}, \tag{19}$$

$$\sin\gamma_{10} = (q_6 x_1 + q_7 x_2 + q_8 x_1^2 + q_9 x_1 x_2 + q_0 x_2^2)/\alpha_{10}, \tag{20}$$

Therefore, eliminating the phase γ_0 from equations (17) and (18) results in an algebraic condition with form

$$f_1(x_1, x_2) \equiv g_7 x_1^3 + g_8 x_1^2 x_2 + g_9 x_1 x_2^2 + g_{10} x_2^3 + g_{11} x_1 x_2 + g_{12} x_2^2 + g_{13} x_2 = 0. \tag{21}$$

Likewise, from the trigonometric identity $\cos^2 \gamma_{10} + \sin^2 \gamma_{10} = 1$ and the equations (19) and (20) it turns out that

$$\begin{aligned} f_2(x_1, x_2) \equiv\ & q_{10} x_1^4 + q_{11} x_1^3 x_2 + q_{12} x_1^2 x_2^2 + q_{13} x_1 x_2^3 + q_{14} x_2^4 \\ & + q_{15} x_1^3 + q_{16} x_1^2 x_2 + q_{17} x_1 x_2^2 + q_{18} x_2^3 + q_{19} x_1^2 + q_{20} x_1 x_2 + q_{21} x_2^2 + q_{22} x_1 = 0. \end{aligned} \tag{22}$$

All the coefficients appearing in equations (17)–(22) are constants, depending on the system parameters. Numerical solution of the last two algebraic equations provides the amplitudes α_{10} and α_{20}. Then, back substitution in (17) and (18) determines the corresponding phase γ_0, while back substitution in (19) and (20) yields the value of γ_{10}. Finally, the phase γ_{20} is evaluated from (14b), which completes the process of determining constant mixed-mode solutions of (8)–(11).

The *stability* properties of a constant mixed-mode solution of equations (8)–(11), say $\mathbf{x}_0 = (\alpha_{10}\ \ \alpha_{20}\ \ \gamma_{10}\ \ \gamma_{20})^{\mathrm{T}}$, are investigated by applying the classical method of linearization [3]. Namely, a small perturbation is first introduced in that solution and a new solution $\mathbf{x} = \mathbf{x}_0 + \varepsilon \mathbf{x}_1$ is considered. Substituting the above expression in (8)–(11), Taylor-expanding around $\mathbf{x}_0$ and keeping only up to linear terms in ε leads to a linear equation with form:

$$\mathbf{x}_1' = \mathbf{\Pi} \mathbf{x}_1, \tag{23}$$

governing the time evolution of the solution perturbation. Then, if the real parts of all the eigenvalues of the constant Jacobian matrix $\mathbf{\Pi}$ are negative, the solution examined is stable. If at least one eigenvalue has positive real part the solution is unstable. Finally, for parameter combinations leading to eigenvalues of matrix $\mathbf{\Pi}$ with zero real part, bifurcations occur [18].

4. PRIMARY RESONANCE OF THE SECOND MODE

When the forcing frequency is close to the linear natural frequency of the second mode of vibration, namely when

$$\omega = \omega_2 + \varepsilon \sigma_2, \tag{24}$$

it can be shown, by applying the same asymptotic procedure as in the previous section, that the amplitudes and phases of approximate solutions expressed by (7) are now determined as solutions of the following set of slow-flow equations:

$$\alpha_1' = c_1 \alpha_1 + c_2 \alpha_1^3 + c_3 \alpha_1 \alpha_2^2 + (c_7 \sin \gamma - c_8 \cos \gamma) \alpha_1^2 \alpha_2, \tag{25}$$

$$\alpha_1 \gamma_1' = \hat{\sigma}_1 \alpha_1 + c_5 \alpha_1^3 + c_6 \alpha_1 \alpha_2^2 + (c_7 \cos \gamma + c_8 \sin \gamma) \alpha_1^2 \alpha_2, \tag{26}$$

$$\alpha_2' = e_1 \alpha_2 + e_2 \alpha_1^2 \alpha_2 + e_3 \alpha_2^3 + e_4 \sin \gamma_2 - (e_7 \sin \gamma + e_8 \cos \gamma) \alpha_1^3, \tag{27}$$

$$\alpha_2 \gamma_2' = \sigma_2 \alpha_2 + e_5 \alpha_1^2 \alpha_2 + e_6 \alpha_2^3 + e_4 \cos \gamma_2 + (e_7 \cos \gamma - e_8 \sin \gamma) \alpha_1^3. \tag{28}$$

Here,

$$\gamma_1 = \hat{\sigma}_1 \tau_1 - \varphi_1, \qquad \gamma_2 = \sigma_2 \tau_1 + \theta_2 - \varphi_2, \tag{29a, b}$$

while the phase γ is defined by (12a) again.

In the present case, it can be proved that equations (25)–(28) possess the same symmetry properties as the averaged equations (8)–(11). However, *single-mode* solutions with

$$\alpha_1 = 0, \qquad \alpha_2 \neq 0,$$

are also possible here. These solutions satisfy equations (25) and (26) identically, while they replace (27) and (28) by:

$$\alpha_2' = e_1\alpha_2 + e_3\alpha_2^3 + e_4 \sin\gamma_2, \qquad \alpha_2\gamma_2' = \sigma_2\alpha_2 + e_6\alpha_2^3 + e_4 \cos\gamma_2. \tag{30a, b}$$

Clearly, these equations are not affected by the presence of the 1:3 internal resonance. In fact, their form is identical to that analyzed for single-mode non-resonant response in [17].

For constant *mixed-mode* solutions of the slow-flow equations (25)–(28), it can first be shown through direct application of (12a) and (29) that

$$\hat{\sigma}_1 = (\sigma + \sigma_2)/3, \qquad \gamma_0 = 3\gamma_{10} - \gamma_{20} + \theta_2. \tag{31a, b}$$

Then, by employing relations (3), (24), (29) and (31), the corresponding solutions of the equations of motion (1) can be expressed in the form

$$u_1 = \alpha_{10} \cos([\omega/3]\tau - \gamma_{10}) + O(\varepsilon) \tag{32}$$

and

$$u_2 = \alpha_{20} \cos(\omega\tau + \theta_2 - \gamma_{20}) + O(\varepsilon). \tag{33}$$

The methodology which leads to determination of the constant mixed-mode solutions of (25)–(28) is similar to that applied in the previous section. Namely, the two algebraic equations resulting from (25) and (26) are first solved for $\cos\gamma_0$ and $\sin\gamma_0$. This yields expressions with form

$$\cos\gamma_0 = (\xi_1 + \xi_2 x_1 + \xi_3 x_2)/\alpha_{10}\alpha_{20}, \qquad \sin\gamma_0 = (\xi_4 + \xi_5 x_1 + \xi_6 x_2)/\alpha_{10}\alpha_{20}. \tag{34, 35}$$

Then, substitution of the last two expressions in the equations arising from (27) and (28) and solution with respect to $\cos\gamma_{20}$ and $\sin\gamma_{20}$, yields

$$\cos\gamma_{20} = (\rho_1 x_1 + \rho_2 x_2 + \rho_3 x_1^2 + \rho_4 x_1 x_2 + \rho_5 x_2^2)/\alpha_{20}, \tag{36}$$

$$\sin\gamma_{20} = (\rho_6 x_1 + \rho_7 x_2 + \rho_8 x_1^2 + \rho_9 x_1 x_2 + \rho_0 x_2^2)/\alpha_{20}. \tag{37}$$

Therefore, employing known trigonometric identities in conjunction with the last four relations leads to a couple of algebraic equations with form

$$f_3(x_1, x_2) \equiv \xi_7 x_1^3 + \xi_8 x_1^2 x_2 + \xi_9 x_1 x_2^2 + \xi_{10} x_1^2 + \xi_{11} x_1 x_2 + \xi_{12} x_1 = 0 \tag{38}$$

and

$$\begin{aligned} f_4(x_1, x_2) \equiv{}& \rho_{10} x_1^4 + \rho_{11} x_1^3 x_2 + \rho_{12} x_1^2 x_2^2 + \rho_{13} x_1 x_2^3 + \rho_{14} x_2^4 \\ &+ \rho_{15} x_1^3 + \rho_{16} x_1^2 x_2 + \rho_{17} x_1 x_2^2 + \rho_{18} x_2^3 + \rho_{19} x_1^2 + \rho_{20} x_1 x_2 + \rho_{21} x_2^2 + \rho_{22} x_2 = 0 \end{aligned} \tag{39}$$

for the two unknowns $x_1 = \alpha_{10}^2$, $x_2 = \alpha_{20}^2$. Again, the constant coefficients in equations (34)–(39) are known functions of the system parameters. Numerical solution of the last two algebraic equations determines the amplitudes α_{10} and α_{20}. Then, the phases γ_0 and γ_{20} are computed from (34), (35) and (36), (37), respectively, while the corresponding phase γ_{10} is evaluated from (31b). Finally, the stability analysis of these solutions is carried out as in the case of primary resonance of the first mode.

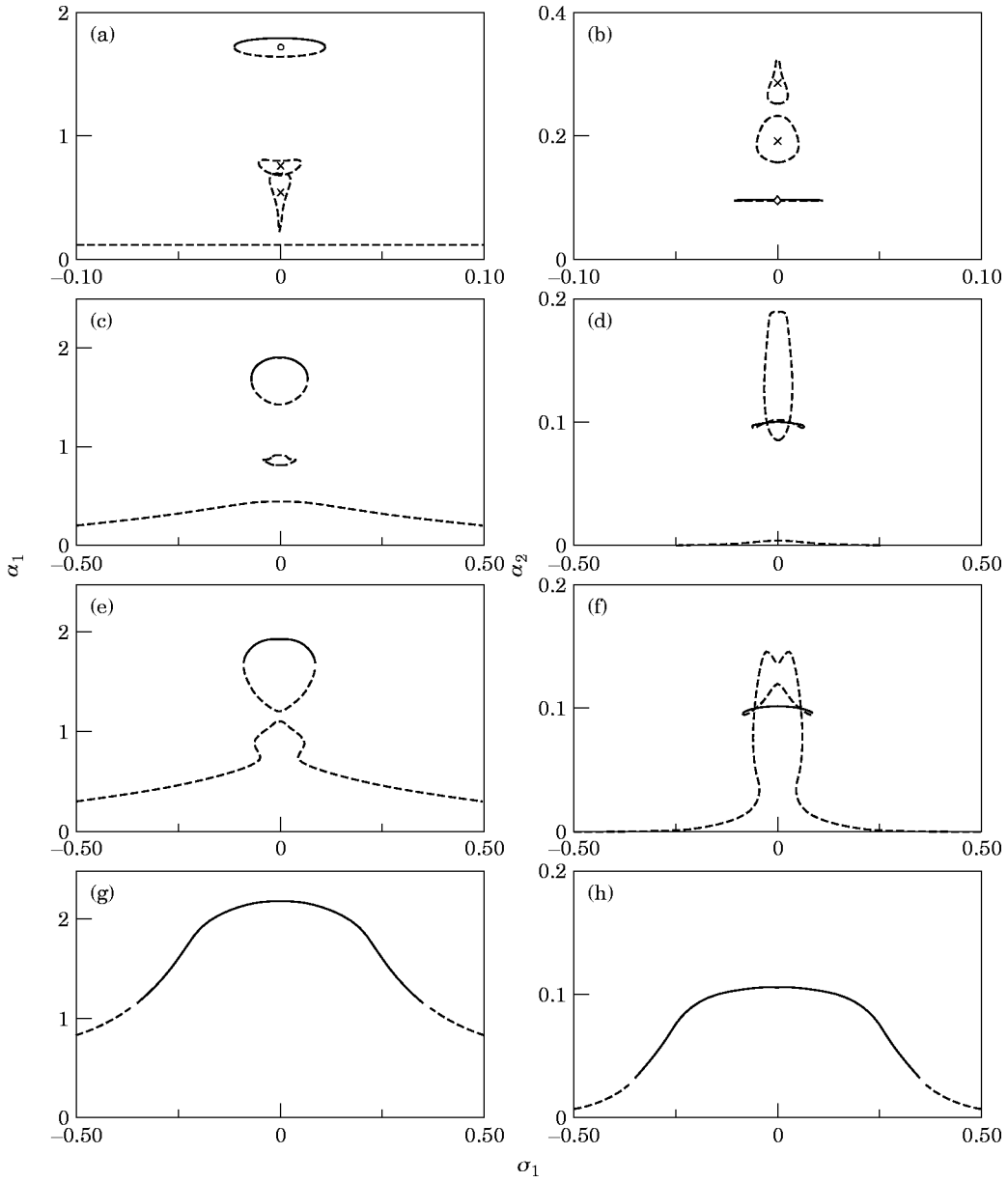

Figure 2. Frequency response diagram of α versus σ_1: (a) α_1 at $f = 0{\cdot}001$; Key: free vibration ($f = 0$); ○, stable solutions; x, unstable solution; ◇, $\alpha_1 = 0$ motion. (b) α_2 at $f = 0{\cdot}001$; Key as for (a). (c) α_1 at $f = 0{\cdot}003$; (d) α_2 at $f = 0{\cdot}003$; (e) α_1 at $f = 0{\cdot}004$; (f) α_2 at $f = 0{\cdot}004$; (g) α_1 at $f = 0{\cdot}01$; (h) α_2 at $f = 0{\cdot}01$.

5. PARAMETRIC STUDY

In this section, numerical results are presented in the form of frequency–response constant solutions. The solution amplitudes are plotted versus the frequency detuning parameter σ_1. Solid lines represent stable solution branches while broken lines represent unstable solution branches. According to relations (15), (16) and the co-ordinate transformation (4), these solutions correspond to two-frequency periodic motions of the mechanical oscillator.

First, Figure 2 shows response diagrams for a system with parameters $\mu = 0{\cdot}6$, $\rho_0 = 0{\cdot}8$, $\zeta_0 = 0{\cdot}01$, $\zeta_1 = \zeta_2 = 0{\cdot}001$, $\sigma = 0$, $\hat{\kappa}_0 = 0$, $\varphi = 0$ and four different values of the forcing parameter $f = f_1 = f_2$. In particular, the isolated points shown in Figures 2(a) and 2(b) correspond to solutions obtained by applying the analysis presented in [19], for the same system but for free vibration (namely, for $f = 0$). The small circles represent stable solutions, the x's correspond to unstable solutions, while the rhombus stands for a motion with $\alpha_1 = 0$. Clearly, as the forcing parameter starts increasing from zero, the original isolated solutions are replaced by closed solution branches which increase in size gradually, collide and merge in a very distinct sequence (Figures 2(c–h)). For values of f larger than 0·01, the form of the response diagrams remains qualitatively the same as that of Figures 2(g) and 2(h). The only significant change caused by a further increase in f is the gradual expansion in the range of stable solutions.

All the response diagrams of Figure 2 appear to be symmetric with respect to the $\sigma_1 = 0$ axis. Next, in obtaining the sequence of response diagrams of Figure 3, the values of the parameters σ and f are set to the constant values 2 and 0·01, respectively, while the value of the stiffness nonlinearity parameter $\hat{\kappa}_0$ is varied. In these cases, the symmetry with respect to the $\sigma_1 = 0$ axis is broken. Moreover, the most important interaction of the

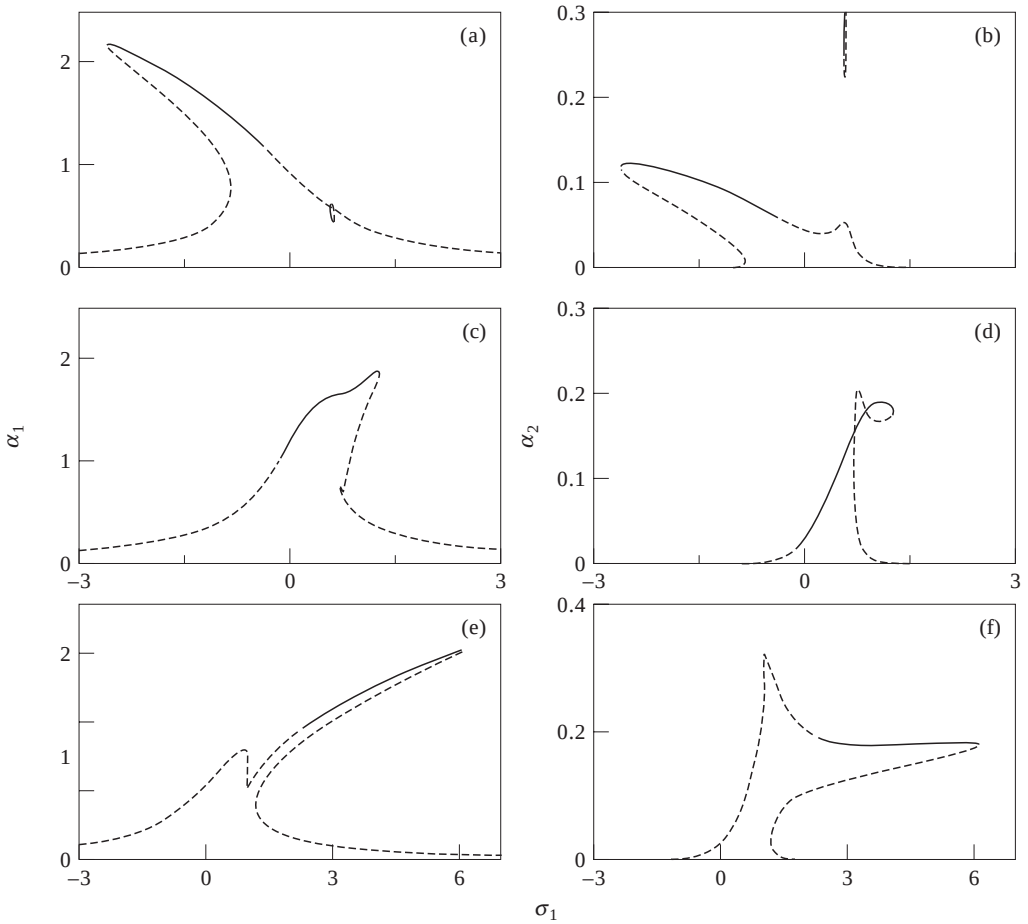

Figure 3. Frequency-response diagram of α versus σ_1: (a) α_1 at $\hat{\kappa}_0 = -2$; (b) α_2 at $\hat{\kappa}_0 = -2$; (c) α_1 at $\hat{\kappa}_0 = 1$; (d) α_2 at $\hat{\kappa}_0 = 1$; (e) α_1 at $\hat{\kappa}_0 = 5$; (f) α_2 at $\hat{\kappa}_0 = 5$.

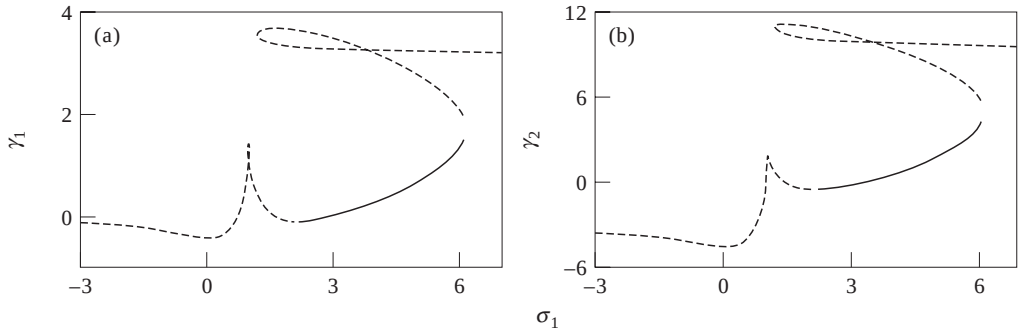

Figure 4. Frequency-response diagram of γ versus σ_1: (a) γ_1 at $\hat{\kappa}_0 = 5$; (b) γ_2 at $\hat{\kappa}_0 = 5$.

constant solution branches takes place in the positive/negative range of the detuning σ_1 for positive/negative values of $\hat{\kappa}_0$, respectively. Finally, for the sake of completeness, Figure 4 depicts the diagrams of the constant phases γ_1 and γ_2, corresponding to the same set of parameters that led to the response diagrams of Figures 3(e) and 3(f).

The response diagrams of Figures 2–4 are typical. Namely, qualitatively similar diagrams were obtained by varying the other technical parameters of the system. The information extracted from such diagrams illustrates the mechanisms giving rise to periodic motions of the dynamical system and provides the means to properly select the system parameters in ways that avoid unwanted motions or reduce their amplitude, within a specified range of interest. In addition, the results of the stability analysis can be used as a guide in order to detect other possible types of motion. For instance, in places where the stability of a branch of constant solutions of the slow-flow equations (8)–(11) is lost through a Hopf bifurcation, these equations accept periodic solutions [18], corresponding to amplitude and phase modulated motions of the mechanical system. This is verified and analyzed further in the following section.

6. NUMERICAL INTEGRATION OF THE SLOW-FLOW EQUATIONS

The branch of stable solutions in Figures 3(e) and 3(f) extends over a relatively narrow frequency range only. As is verified by the numerical results of the stability analysis, this branch coalesces at its right end with a branch of unstable constant solutions, through a saddle–node bifurcation. On the other hand, the stability at its left end is lost through a Hopf bifurcation at about $\sigma_1 = 2{\cdot}29$. By direct integration of the slow-flow equations (8)–(11) it is confirmed that these equations exhibit stable periodic solutions in the range extending from $\sigma_1 = 2{\cdot}32$ to $1{\cdot}42$, showing that the Hopf bifurcation is subcritical. Within that frequency range, the projections of the longtime response onto the (α_1, α_2) plane appear in the forms shown in Figure 5.

In Figure 5(a), two different periodic solutions (obtained at $\sigma_1 = 1{\cdot}55$) are shown, which are mirror images with respect to the $\alpha_2 = 0$ axis. This is due to the symmetry property $(\alpha_1, \alpha_2, \gamma_1, \gamma_2) \rightarrow (\alpha_1, -\alpha_2, \gamma_1, \pi + \gamma_2)$. These twin trajectories are known as Rossler attractors [7]. By further decreasing the value of the forcing detuning parameter, the two twin attractors of the (α_1, α_2) plane move closer to the $\alpha_2 = 0$ axis and eventually collide at a critical value of σ_1, forming a single Lorenz attractor. They then remain connected within a forcing frequency range, as shown in Figures 5(b) and 5(c). Finally, for even smaller values of σ_1 the Lorenz attractor separates and forms two new twin Rossler attractors, as shown in Figure 5(d).

The types of solutions shown in Figure 5 have also been observed in previous studies of non-linear dynamical systems (e.g., [18–22]). In those studies, the existence of solutions similar to those shown on Figure 5 was related to the satisfaction of some special dynamical conditions, resulting in the so-called Silnikov phenomena. These conditions ensure the existence of a saddle-focus constant solution of the slow-flow equations, which possesses a bi-asymptotic homoclinic orbit [18, 20]. In the case examined, the eigenvalues of the linear part of the averaged equations at $\sigma_1 = 1{\cdot}504$ are: $\lambda_{1,2} = 0{\cdot}067 \pm 1{\cdot}687\mathrm{i}$, $\lambda_3 = -0{\cdot}683$ and $\lambda_4 = 1{\cdot}107$. This provides numerical evidence for the existence of a saddle-focus. Moreover, it indicates satisfaction of the condition for the occurrence of a homoclinic explosion [21], providing justification for the existence of the motions of Figure 5.

The frequency content of the solutions presented in Figure 5 is assessed by the corresponding Fourier spectra, shown in Figure 6. First, Figure 6(a) verifies that the response history $\alpha_2(\tau)$ is periodic at $\sigma_1 = 1{\cdot}55$, before the merging of the two asymmetric Rossler attractors. Following the collision of these attractors and the appearance of the Lorenz attractor, the spectrum of $\alpha_2(\tau)$ starts presenting a continuous distribution of the response energy in the low frequency range (Figure 6(b)), which becomes pronounced (Figure 6(c)), indicating chaotic response. Finally, for even smaller values of σ_1, the response history of the solution amplitude α_2 regains its periodicity, as verified by Figure 6(d).

In order to better understand the dynamics of the system within the frequency range examined, Figure 7 presents the time histories of the phase γ_2 for exactly the same set of values of σ_1. Following the Hopf bifurcation of the stable constant solutions, the phase γ_2 (as well as the phase γ_1 and the solution amplitudes α_1 and α_2) is found to vary periodically within the interval $1{\cdot}51 < \sigma_1 < 2{\cdot}32$, as shown in Figure 7(a). However, within the range of σ_1 where the Lorenz attractor appears onto the (α_1, α_2) plane, the history of phase γ_2 is characterized by sudden jumps. These jumps occur at a low frequency rate originally (Figure 7(b)), which increases quickly (Figure 7(c)). The final result of these

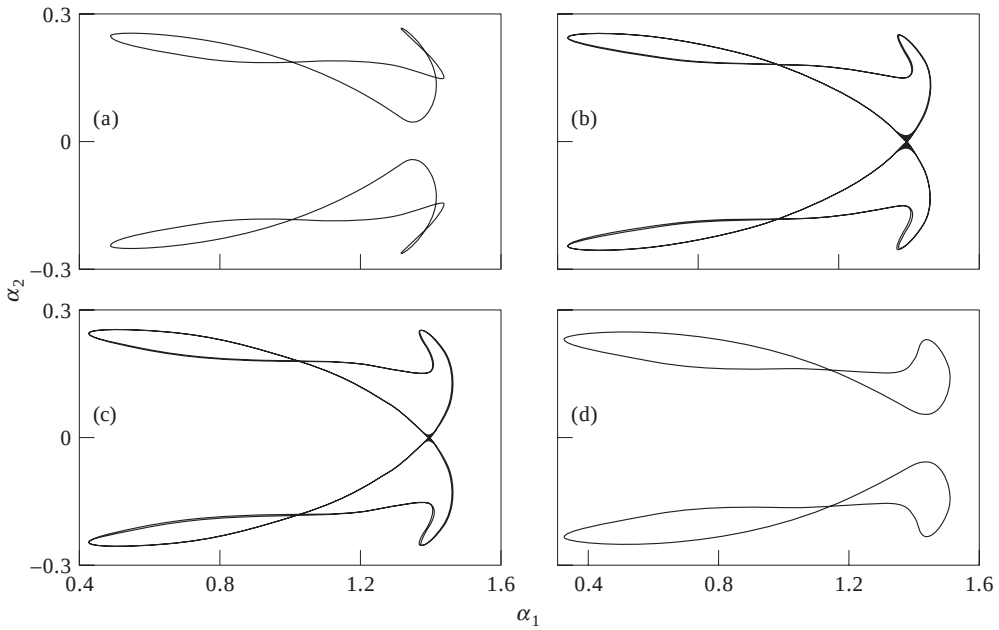

Figure 5. Projection of long time response onto (α_1, α_2) plane, σ_1 values: (a) 1·55, (b) 1·506, (c) 1·504, (d) 1·45.

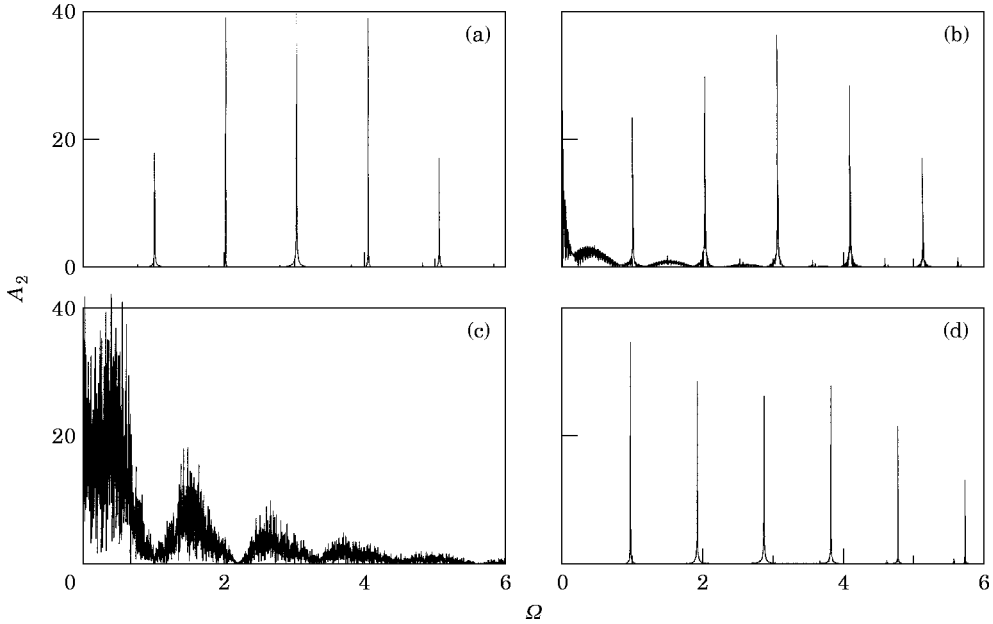

Figure 6. Fourier spectrum of amplitude α_2, σ_1 values: (a) 1·55, (b) 1·506, (c) 1·504, (d) 1·45.

changes is shown in Figure 7(d), where the phase γ_2 exhibits jumps continuously. These results demonstrate that the phase-locked motion, corresponding to the stable constant solutions of the slow-flow equations for $\sigma_1 > 2{\cdot}29$, is originally replaced by entrained motion, corresponding to periodic solutions of the slow-flow equations (see [15] for relevant definitions). At the critical value of σ_1 where the two Rossler attractors collide and form the Lorenz attractor onto the (α_1, α_2) plane, the phase γ_2 starts developing a drift, which is completed when the Lorenz attractor splits apart again.

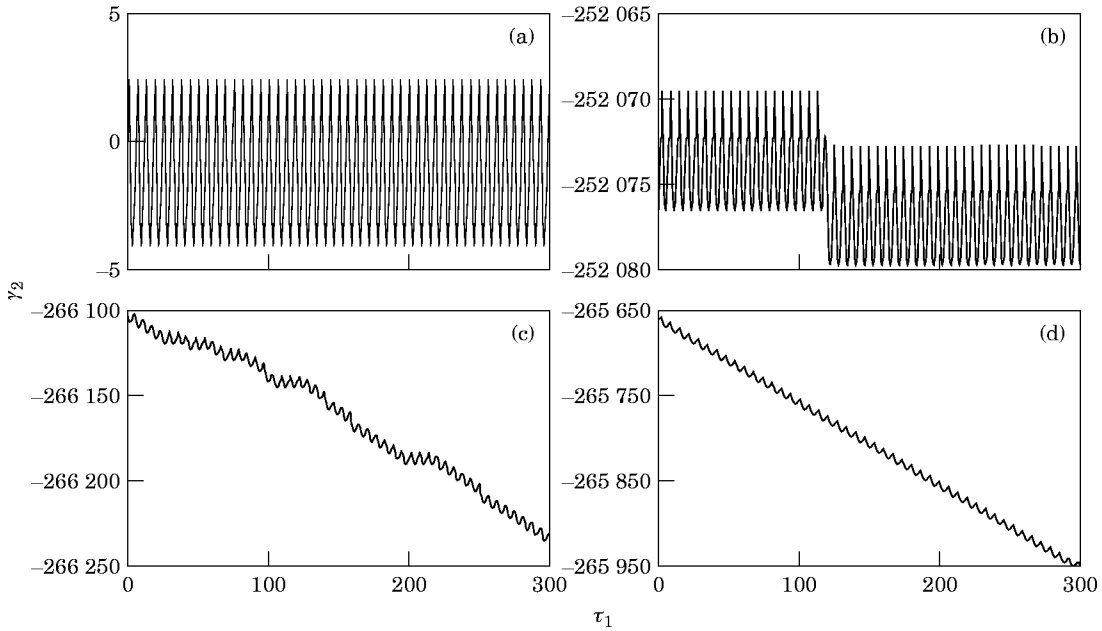

Figure 7. Long time history of phase γ_2, σ_1 values: (a) 1·55, (b) 1·506, (c) 1·504, (d) 1·45.

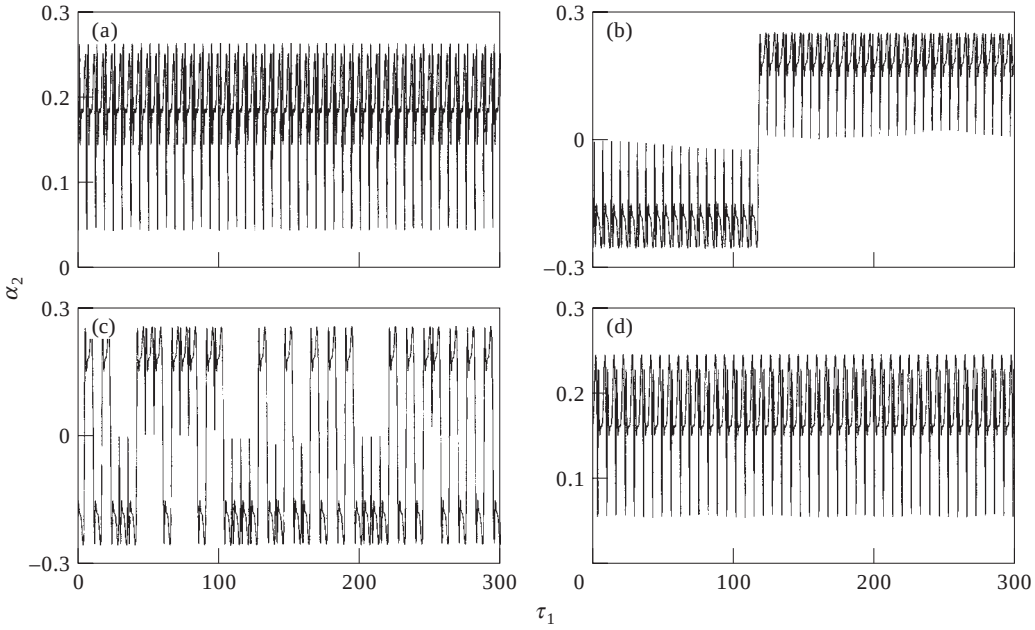

Figure 8. Long time history of amplitude α_2, σ_1 values: (a) 1·55, (b) 1·506, (c) 1·504, (d) 1·45.

Figure 8 shows the history diagrams of the solution amplitude α_2, obtained for the same set of values of the forcing frequency. Clearly, it appears that anytime there is a jump in the history of phase γ_2, a sign change occurs in the history of α_2, until the system has reached the state of full drift. This result is in accordance with the aforementioned symmetry property of the averaged equations. On the other hand, the corresponding response histories $\alpha_1(\tau_2)$ and $\gamma_1(\tau_1)$ were found to remain periodic throughout the frequency range considered, even when the history of amplitude α_2 is chaotic. This curious result is illustrated by Figure 9, obtained at $\sigma_1 = 1{\cdot}504$.

It should be pointed out that the solutions belonging to the same sequence with those shown in Figure 5 become unstable eventually at about $\sigma = 1{\cdot}415$, where the direct integration converges to another coexisting periodic solution. This new solution is shown in Figure 10 for two values of σ_1 and was found to exist in the interval extending from $\sigma_1 = 1{\cdot}8$ to -20. A special characteristic of this solution is that both of its phases γ_1, γ_2 are in a condition of full drift.

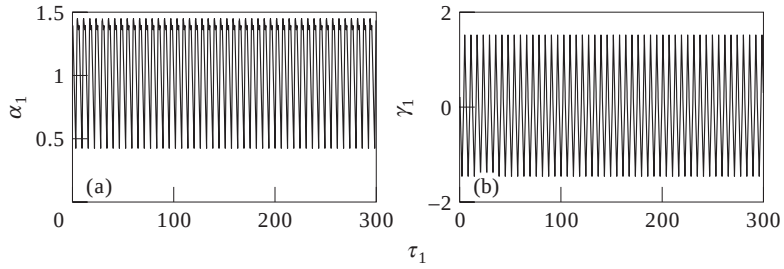

Figure 9. Long time history of amplitude α_1 with $\sigma_1 = 1{\cdot}504$; (a) α_1, (b) γ_1.

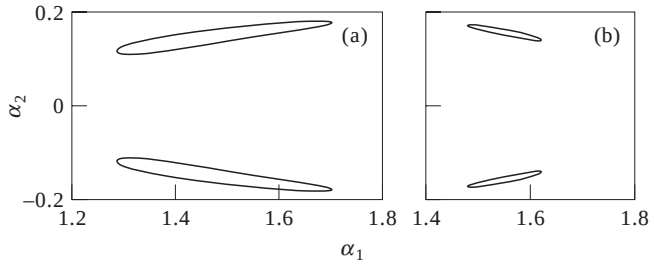

Figure 10. Projection of long time response onto (α_1, α_2) plane σ_1 values; (a) 1·41, (b) -5.

7. SUMMARY AND CONCLUSIONS

An analysis has been presented for predicting the dynamic behavior of two-degree-of-freedom symmetric self-excited systems, in the presence of 1:3 internal resonance and the simultaneous action of external primary resonances. First, sets of slow-flow equations were obtained for the amplitudes and phases of approximate asymptotic motions of the system. Determination of constant solutions of these equations was reduced to solution of two coupled polynomial equations. These solutions were shown to correspond to periodic motions of the system and their stability characteristics were investigated by the method of linearization. Then, series of representative response diagrams were presented for constant solutions, illustrating the dependence of their existence and stability properties on the system parameters. Finally, a search was performed in forcing frequency ranges where no stable constant solutions are possible. By performing numerical integration, a scenario leading to a gradual transition from phase-locked to drift solutions of the slow-flow equations was revealed, corresponding to a transition from periodic to quasiperiodic response of the original system. This transition started with a subcritical Hopf bifurcation and was reinforced by satisfaction of Silnikov conditions, leading to a homoclinic explosion of the averaged equations. In addition, it involved the appearance of chaotic response of the directly excited mode only, as was confirmed by phase-planes, response histories and Fourier spectra. Finally, the direct integration showed the coexistence of another solution branch of the slow-flow equations, having both of its phases in a condition of full drift, over a forcing frequency interval.

REFERENCES

1. J. C. Chen and C. D. Babcock 1972 *American Institute of Aeronautics and Astronautics Journal* **13**, 868–876. Nonlinear vibration of cylindrical shells.
2. P. R. Sethna and A. K. Bajaj 1978 *Journal of Applied Mechanics* **45**, 895–902. Bifurcations in dynamical systems with internal resonance.
3. A. H. Nayfeh and D. T. Mook 1979 *Nonlinear Oscillations*. New York: Wiley-Interscience.
4. J. W. Miles 1984 *Journal of Fluid Mechanics* **149**, 15–31. Resonantly forced surface waves in a circular cylinder.
5. D. T. Mook, R. H. Plaut and N. HaQuang 1985 *Journal of Sound and Vibration* **102**, 473–492. The influence of an internal resonance on nonlinear structural vibrations under subharmonic resonance conditions.
6. A. H. Nayfeh and B. Balachandran 1989 *Applied Mechanics Review* **42**, 175–201. Modal interactions in dynamical and structural systems.
7. J. M. Johnson and A. K. Bajaj 1989 *Journal of Sound and Vibration* **128**, 87–107. Amplitude modulated and chaotic dynamics in resonant motion of strings.
8. S. Natsiavas 1994 *International Journal of Nonlinear Mechanics* **29**, 31–48. Dynamics and stability of non-linear free vibration of thin rotating rings.

9. C. HAYASHI and M. KURAMITSU 1974 *Memoirs of the Faculty of Engineering Kyoto University* **36**, 87–104. Self-excited oscillations in a system with two degrees of freedom.
10. W. D. IWAN and R. D. BLEVINS 1974 *Journal of Applied Mechanics* **41**, 581–586. A model for vortex induced oscillation of structures.
11. A. TONDL 1976 *On the interaction between self-excited and forced vibrations*. Prague: National Research Institute for Machine Design.
12. E. I. RIVIN and H. KANG 1989 *International Journal of Machine Tools and Manufacturing* **29**, 361–376. Improvement of machining conditions for slender parts by tuned dynamic stiffness of tool.
13. A. MUSZYNSKA 1986 *Journal of Sound and Vibration* **110**, 443–462. Whirl and whip rotor/bearing stability problems.
14. J. SHAW and S. W. SHAW 1989 *Journal of Sound and Vibration* **132**, 227–244. Instabilities and bifurcations in a rotating shaft.
15. T. CHAKRABORTY and R. H. RAND 1988 *International Journal of Nonlinear Mechanics* **23**, 369–376. The transition from phase locking to drift in a system of two weakly coupled van der Pol oscillators.
16. S. NATSIAVAS 1994 *Nonlinear Dynamics* **6**, 69–86. Free vibration of two coupled oscillators.
17. S. NATSIAVAS 1995 *Journal of Sound and Vibration* **184**, 261–280. Modal interactions in self-excited oscillators under external primary resonance.
18. S. WIGGINS 1990 *Introduction to Applied Nonlinear Dynamical Systems and Chaos*. New York: Springer-Verlag.
19. S. NATSIAVAS, K. D. BOUZAKIS and P. AICHOUH 1997 *Nonlinear Dynamics* **12**, 109–128. Free vibration in a class of self-excited oscillators with 1:3 internal resonance.
20. P. GASPARD, R. KAPRAL and G. NICOLIS 1984 *Journal of Statistical Physics* **35**, 697–727. Bifurcation phenomena near homoclinic systems: a two-parameter analysis.
21. O. M. O'REILLY 1993 *International Journal of Nonlinear Mechanics* **28**, 337–351. Global bifurcations in the forced vibration of a damped string.
22. S. SAMARANAYAKE, A. K. BAJAJ and O. D. I. NWOKAH 1995 *Acta Mechanica* **109**, 101–125. Amplitude modulated dynamics and bifurcations in the resonant response of a structure with cyclic symmetry.

APPENDIX: DEFINITION OF SOME PARAMETERS

$$\mu = m_2/m_1, \qquad m_0 = m_2, \qquad \hat{\omega}_n = \sqrt{k_n/m_n}, \qquad \zeta_n = c_n/(2\sqrt{k_n m_n}), \qquad (n = 0, 1, 2)$$

$$\rho = \frac{\hat{\omega}_2}{\hat{\omega}_1}, \qquad \rho_0 = \frac{\hat{\omega}_0}{\hat{\omega}_1}, \qquad \varepsilon = 2\mu\rho_0\zeta_0, \qquad x_c = \sqrt{\frac{m_1 c_0}{3k_1\hat{c}_0}}, \qquad \varepsilon\hat{\kappa}_0 = \frac{\hat{k}_0}{k_1}x_c^2, \qquad f_n = \frac{F_n}{k_1 x_c}$$

$$2\varepsilon p_n = \sqrt{(y_{1n}f_1 + y_{2n}f_2\cos\varphi)^2 + (y_{2n}f_2\sin\varphi)^2}, \qquad \tan\theta_n = \frac{y_{2n}f_2\sin\varphi}{y_{1n}f_1 + y_{2n}f_2\cos\varphi} \qquad (n = 1, 2)$$

$$c_1 = \frac{\alpha_{11}}{2}, \qquad c_2 = \frac{3\beta_{11}}{8}\omega_1^2, \qquad c_3 = \frac{\beta_{13}}{4}\omega_2^2, \qquad c_4 = \frac{p_1}{\omega_1}, \qquad c_5 = \frac{3\gamma_{11}}{8\omega_1},$$

$$c_6 = \frac{\gamma_{13}}{4\omega_1}, \qquad c_7 = \frac{\gamma_{12}}{8\omega_1}, \qquad c_8 = \frac{\beta_{12}}{8}\omega_1\omega_2,$$

$$e_1 = \frac{\alpha_{22}}{2}, \qquad e_1 = \frac{\beta_{22}}{4}\omega_1^2, \qquad e_3 = \frac{3\beta_{24}}{8}\omega_2^2, \qquad e_4 = \frac{p_2}{\omega_2}, \qquad e_5 = \frac{\gamma_{22}}{4\omega_2},$$

$$e_6 = \frac{3\gamma_{24}}{8\omega_2}, \qquad e_7 = \frac{\gamma_{21}}{8\omega_2}, \qquad e_8 = \frac{\beta_{21}}{8\omega_2}\omega_1^3$$

$$\delta_1 = \tfrac{1}{8}\nu_{11}\alpha_1^3 + \tfrac{1}{4}\nu_{15}\alpha_1\alpha_2^2 + \tfrac{1}{8}[(\omega_2\mu_{13} - \omega_1\mu_{12})\sin\gamma + (\nu_{12}\omega_2/\omega_1 - \nu_{13})\cos\gamma]\alpha_1^2\alpha_2,$$

$$\delta_2 = \tfrac{1}{8}\omega_1\mu_{11}\alpha_1^3 + \tfrac{1}{4}\omega_2^2/\omega_1\mu_{15}\alpha_1\alpha_2^2 + \tfrac{1}{8}[(\omega_2\mu_{13} - \omega_1\mu_{12})\cos\gamma + (\nu_{13} - \omega_2/\omega_1\nu_{12})\sin\gamma]\alpha_1^2\alpha_2,$$

$$\delta_3 = \tfrac{1}{4}\nu_{22}\alpha_1^2\alpha_2 + \tfrac{1}{8}\nu_{26}\alpha_2^3 + \omega_1/(8\omega_2)(\omega_1\mu_{21}\sin\gamma + \nu_{21}\cos\gamma)\alpha_1^3,$$

$$\delta_4 = \tfrac{1}{4}\omega_1^2/\omega_2\mu_{22}\alpha_1^2\alpha_2 + \tfrac{1}{8}\omega_2\mu_{26}\alpha_2^3 - \omega_1/(8\omega_2)(\omega_1\mu_{21}\cos\gamma - \nu_{21}\sin\gamma)\alpha_1^3.$$